UNIVERSITEIT VAN AMSTERDAM

VU VRIJE UNIVERSITEIT AMSTERDAM

Tensor network study of the 2D Blume-Capel model

Derk Niessink

Report Bachelor Project Physics and Astronomy, 15 EC
Conducted between 02-04-2023 and 07-07-2023

Institute for Theoretical Physics Amsterdam
Faculteit der Natuurwetenschappen, Wiskunde en Informatica

Student-ID	13438921
Date of Submission	07-07-2023
Supervisor	Dr. P.R. Corboz
Daily Supervisor	Y. Zhang MSc
Examiner	Dr. E. Lerner

Abstract

The Blume-Capel model is used in statistical physics to simulate magnetic materials. It is one of the simplest lattice models that exhibits a tricritical point in the phase diagram. This model serves as an extension of the Ising model by introducing the additional spin state 0 and including the zero-field splitting term into the Hamiltonian. The partition function of the Blume-Capel model for a 2D square lattice can be represented as a 2D network of rank-4 tensors. These tensors can be efficiently evaluated using the Corner Transfer Matrix Renormalization Group (CTMRG) method and the accuracy can be systematically controlled by the so-called bond dimension χ.

In this study, the CTMRG method is used to compute thermodynamic properties such as magnetization per site, free energy, correlation length, heat capacity, and magnetic susceptibility for both the Blume-Capel and Ising model. The phase diagram of the Blume-Capel model is presented, along with a comparison of its accuracy to recent studies. The accuracy in the first order regime is improved by three decimal points, while achieving similar accuracy as recent works in the second order regime. An estimate for the tricritical point is presented, $[\Delta_t = 1.96600(1), T_t = 0.6079(1)]$, which agrees with recent studies and provides an improvement in accuracy for Δ_t of one decimal point.

Populair wetenschappelijke samenvatting

Het *Blume-Capel model* is een eenvoudig model dat wordt gebruikt om de gedragingen van magnetische materialen te bestuderen. Stel je een rooster voor waarin elk punt een klein magneetje kan hebben dat naar boven of naar beneden wijst. Dit rooster representeert een rooster van atomen, die bepaalde spins en daardoor magnetische dipool momenten hebben. In het Blume-Capel model kan een magneetje alleen communiceren met zijn directe buren.

Het idee achter de Blume-Capel model is om te zien hoe deze magneten op elkaar inwerken en hoe ze zich gedragen bij verschillende temperaturen. Bij hoge temperaturen zijn de magneten chaotisch en wijzen ze in willekeurige richtingen. Bij lage temperaturen hebben de magneten de neiging om zich te ordenen en wijzen ze vaak allemaal naar dezelfde richting. Deze overgang van de geordende naar de chaotische staat, noemen we een *fase-overgang*. Het Blume-Capel model helpt ons te begrijpen hoe deze fase-overgang plaatsvindt.

Een grafiek die de grens laat zien tussen twee fases, noemen we een *fase diagram*. In mijn project heb ik deze fase diagram gereconstrueerd, door te bepalen bij welke temperaturen de fase-overgang plaatsvindt, *de kritische temperaturen*. Deze temperaturen kunnen berekend worden met behulp van een computer simulatie. Dit kan op veel verschillende manieren, maar zo'n simulatie kost al snel veel computerkracht. Ik heb daarom een nieuwe efficiente methode gebruikt om het model te simuleren, genaamd *The Corner Transfer Matrix Renormalization Group method* (afgekort CTMRG methode).

We representeren eerst het rooster als een netwerk van tensoren. Een *tensor* is een generalisatie van een matrix, en is gedefinieerd als een wiskundig object dat in meerdere dimensies getallen kan opslaan. De CTMRG methode maakt het nu mogelijk om een oneindig netwerk van tensoren te benaderen met een eindig netwerk. Met het resultaat van de CTRMG methode kunnen thermodynamische eigenschappen van een oneindig systeem worden berekend. Uit deze eigenschappen heb ik de kritische temperaturen bepaald en de fase diagram kunnen construeren. Mijn resultaten heb ik vergeleken met wetenschappelijke artikelen die ook het Blume-Capel model hebben bestudeerd, maar met andere methodes. Ik heb een verbetering in precisie van ongeveer drie decimalen kunnen behalen voor de kritische temperaturen in de fase diagram. Dit laat zien dat de CTMRG methode een zeer krachtig methode is voor het simuleren van het Blume-Capel model.

Contents

1 Introduction

Models of matter that are defined as many-body problems are of great interest due to their ability to exhibit emergent phenomena such as phase transitions and superconductivity. However, the numerical evaluation of these models faces a significant challenge due to the computational cost associated with simulating the interactions between particles. The number of particle configurations grows exponentially with system size. To address this issue, an efficient approach involves representing the partition function of a system as tensor networks. The Corner Transfer Matrix Renormalization Group (CTMRG) method [1] offers an effective means to evaluate infinite systems composed of identical tensors in a network with relatively low computational cost. The accuracy of the approximation of the system can be controlled with the bond dimension χ, which is a parameter that controls the size of the tensors in the network. The leading computational cost of the CTMRG method is $\mathcal{O}(\chi^3)$. Originally introduced as a technique for evaluating 2D classical systems, the CTMRG method has proven to be a valuable tool in this context, and especially in the study of quantum many-body systems [2].

The goal of this thesis is to investigate two classical 2D spin systems using the CTMRG method, and compare the obtained results with exact solutions and recent studies conducted on these particular models. The first model studied in this work is the Ising model, which serves as one of the simplest lattice models that exhibits a phase transition between the paramagnetic and ferromagnetic states. Despite its simplicity, the Ising model exhibits interesting behavior relevant to the comprehension of phase transitions in magnetic materials. Therefore, it has been widely studied since it was introduced by Wilhelm Lenz in 1920 [3] and solved by Ernst Ising in 1925 [4].

The second model explored in this work is an extension of the Ising model with the addition of the zero spin state, the Blume-Capel model. This model was initially proposed in the context of magnetic materials [5, 6] and was later found to be applicable to mixtures of ^{3}He and ^{4}He [7]. The model's phase diagram exhibits a phase boundary consisting of a first and second order transition. The tricritical point, located on this phase boundary, marks the boundary between the first and second order transitions.

The structure of the thesis is as follows: Chapter 2 provides the theoretical background on the two models and presents the methodology for representing the partition functions as tensor networks and how to efficiently represent them in graphical notation. Chapter 3 outlines the CTMRG method employed for evaluating the partition functions, as well as the techniques used for computing thermodynamic properties, critical exponents, and, specifically for the Blume-Capel model, the approach for determining the tricritical point. The obtained results for both models are presented in Chapter 4. Lastly, Chapter 5 discusses the findings for both models, with a specific focus on comparing the results of the Ising model to exact solutions and the results of the Blume-Capel model to recent studies conducted on that particular model.

2 Theory

This chapter discusses the theoretical aspects of the two models, the Ising model and the Blume-Capel model. Their Hamiltonians are defined and emergent features explored in Section 2.1 and Section 2.2 respectively. Next, the concept of tensor networks and how to efficiently represent them using graphical notation are covered. Moving on, the partition function for the Ising model is examined and rewritten as an infinite network of identical tensors in Section 2.4. Some modifications to this tensor network are made in Section 2.5 to account for the Blume-Capel model. Finally, in Section 2.6, the behavior and relationships of thermodynamic properties and critical temperatures are investigated, specifically in systems of finite size.

2.1 The Ising model

The Ising Model is a model in statistical physics that is defined by sites that can be either in spin state 1 or -1. The sites represent the up and down magnetic dipole moments produced by atomic spins and interact in a lattice. The 2D Ising model has been widely studied, because it is one of the simplest lattice models that exhibits a phase transition. The model is defined by the following Hamiltonian:

$$\mathcal{H} = -J \sum_{<ij>} \sigma_i \sigma_j - h \sum_i \sigma_i, \tag{1}$$

where $J > 0$ is the ferromagnetic exchange interaction, $\langle ij \rangle$ indicates the sum over all nearest neighbours and σ_i is the spin variable which can be either 1 or -1. Consequently, spins that agree (i.e. point in the same direction), contribute a negative energy and spins that disagree a positive energy to the Hamiltonian. The second term is the energy contribution from an external magnetic field interaction, where h controls the strength of the field. At zero temperature, the system is in its lowest energy state, which is characterized by an alignment of all spins. This alignment can be disturbed by adding heat to the system, leading to an increase in energy. This dependence on temperature is reflected in the system's partition function:

$$Z = \sum_s e^{-\beta \mathcal{H}_s}, \tag{2}$$

where $\beta = 1/k_B T$ in which k_B is the Boltzmann constant and T the temperature and s indicates the summation over all possible energy configurations.

Various thermodynamic properties can be calculated, when the partition function of a system is known. One important property is the magnetization per site, denoted as $m(\beta)$, which represents the average value of the spin state (s_r) at a specific location (lattice site r). It can be expressed as:

$$m(\beta) = \langle s_r \rangle = \left| \frac{\sum_s s_r e^{-\beta \mathcal{H}_s}}{Z} \right|. \tag{3}$$

Another thermodynamic property is the free energy and is given by:

$$f = \frac{-k_B T \ln(Z)}{N}, \tag{4}$$

where N is the number of lattice sites. The exact solution [8] of the magnetization per site is given by

$$m(\beta) = \begin{cases} [1 - \sinh^{-4}(2\beta J)]^{\frac{1}{8}}, & T \leq T_c \\ 0, & T > T_c, \end{cases} \tag{5}$$

where T_c is defined as the critical temperature of the phase transition. For $T \leq T_c$, the system resides in the ferromagnetic (F) state, characterized by an ordered alignment of the spins, and for $T > T_c$, the system exhibits a paramagnetic state, where all spins are randomly aligned.

2.2 The Blume-Capel model

The Blume-Capel model is a generalization of the Ising model that allows spins to take on three possible values: -1, 0, and 1. The key-feature of the Blume-Capel model is the addition of the zero-field splitting term, which introduces an energy difference between the states with spin values of ± 1 and the state with spin value 0. The Blume-Capel Hamiltonian is given by:

$$\mathcal{H} = -J \sum_{<ij>} \sigma_i \sigma_j - h \sum_i \sigma_i + \Delta \sum_i \sigma_i^2, \tag{6}$$

where Δ is the crystal-field coupling parameter. It is important to note that the third term in the equation, known as the zero-field splitting term, introduces a positive energy penalty whenever the spin variables σ_i take on values of ± 1. Thus, Δ controls the proportion of spin 0 states within the system. For $\Delta \to -\infty$ the model reduces to the Ising model (Equation 1), because the energy difference between the 0 state and the ± 1 states approaches ∞ and thus the spin variables will never be in spin state 0.

In the Ising model, the phase boundary only exhibits a second-order (continuous) phase transition between the paramagnetic (P) and ferromagnetic (F) phase. This type of transition is characterized by an infinite correlation length. Further details regarding the behavior near the critical point for the second order phase transition will be discussed in Section 2.6. The Blume-Capel model allows for the construction of a phase diagram in the Δ, T plane, which marks the boundary between the paramagnetic and ferromagnetic phase. A schematic representation of the phase diagram, along with its characteristics, is depicted in Figure 1.

The paramagnetic phase can be either in a completely disordered arrangement of ± 1 spins for high T, or in a state that is dominated by 0 spins with few ± 1 spins for low T and high Δ. The phase transition in this model consists of both a second order transition, at high T, and a first order transition, at low T and high Δ. The point where the two segments of the phase transition meet is referred to as the tricritical point (Δ_t, T_t). At zero temperature, it is clear that for $\Delta > 2J$ the system exists in the paramagnetic phase, as the penalty Δ for having all spins in the ± 1 states exceeds the interaction energy $2J$ per spin. This means that $(\Delta_0 = 2J, T = 0)$ is a point on the phase boundary.

A first-order phase transition is characterized by a discontinuous change in thermodynamic properties. When crossing the phase boundary of the first-order transition, the phenomenon of hysteresis becomes apparent. Hysteresis refers to the state of the system being influenced by its recent history. Crossing the phase boundary from either side, yields distinct solutions and becomes apparent in the free energy of the system.

The 2D Blume-Capel model is one of the simplest lattice models that exhibits a tricritical point in the phase diagram. As a result, this model has been subject of many studies using a diverse range of methodologies, including Monte Carlo (MC) simulations [9, 10, 11], Wang-Landau simulations [12, 13], and phenomenological finite size scaling analysis [14]. The goal of this work is to compare the findings obtained through the application of the CTRMG method to the results reported in these studies.

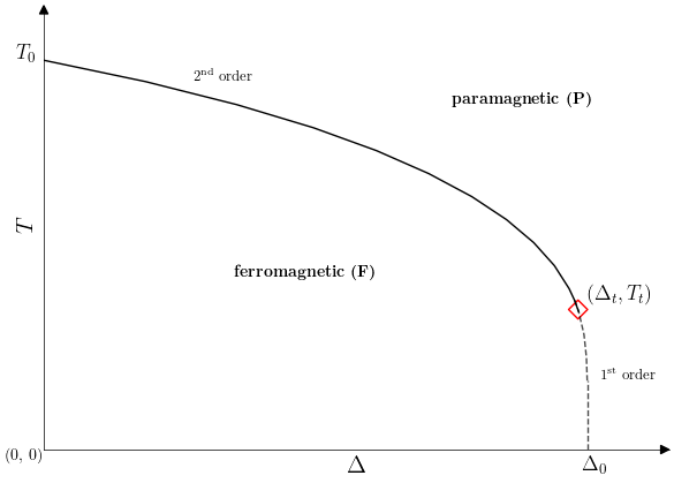

Figure 1: Schematic representation of the phase diagram of the Blume-Capel model in the Δ, T plane. The phase boundary separates the ferromagnetic (F) and paramagnetic (P) phases. The second and first order transition are indicated with the solid and dotted line, respectively. The tricritical point (Δ_t, T_t), the point where the two segments of the phase boundary meet, is indicated by the red diamond.

2.3 Tensor networks and contraction

Tensors provide a mathematical framework for solving problems in physics and can be seen as a generalization of matrices. A scalar, vector and matrix are respectively rank-0, 1, and 2 tensors. Examples of the graphical notation of rank-0, 1, 2, and 3 tensors are shown in Figure 2. The rank of a tensor is equivalent to the number of open legs (i.e indices).

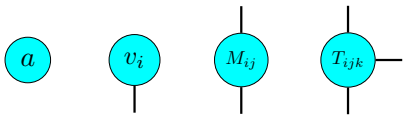

Figure 2: From left to right: tensor network representation of a scalar a, vector v_i, matrix M_{ij} and tensor T_{ijk}, i.e. respectively a rank-0, 1, 2 and 3 tensor.

Tensors with one or more common legs can be contracted. An example of the contraction of two rank-1 tensors and two rank-2 tensors with one common leg are shown in Figure 3, which are respectively equivalent to the vector dot product and matrix multiplication. A tensor network consists of multiple connected nodes, such that there is a path from any node to any other node in the network and it can always be contracted to one tensor with a rank equal to the number of open legs in the network.

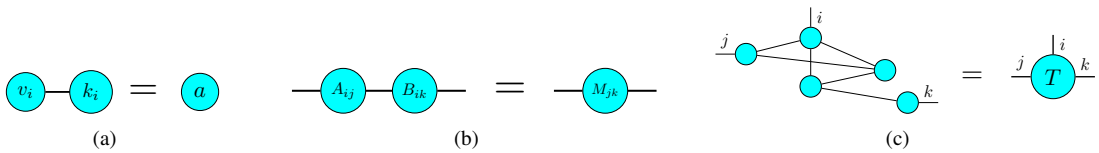

Figure 3: Examples of tensor network contraction: (a) contraction equivalent to a vector dot product: $\sum_i v_i k_i = a$, (b) a matrix multiplication: $\sum_i A_{ij} B_{ik} = M_{jk}$, and (c) a general tensor network contraction to a rank-3 tensor.

2.4 Tensor network representation of the partition function for the Ising model

To represent the Ising model partition function as a tensor network it is convenient to write Equation 2 as a product of two Boltzmann factors; the nearest neighbour and magnetic field interaction. Substituting Equation 1 in Equation 2 gives:

$$Z(\beta) = \sum_s e^{\beta J \sum_{<ij>} \sigma_i \sigma_j + \beta h \sum_i \sigma_i} = \sum_s \prod_{<i,j>} e^{\beta J \sigma_i \sigma_j} \prod_i e^{\beta h \sigma_i}. \tag{7}$$

The Boltzmann factor for the neighbouring interaction contains two indices and can be defined as a matrix:

$$e^{\beta J \sigma_i \sigma_j} = Q_{\sigma_i, \sigma_j} \equiv \begin{pmatrix} Q_{+1,+1} & Q_{+1,-1} \\ Q_{-1,+1} & Q_{-1,-1} \end{pmatrix} = \begin{pmatrix} e^{\beta J} & e^{-\beta J} \\ e^{-\beta J} & e^{\beta J} \end{pmatrix} \tag{8}$$

The external magnetic field interaction product contains one index and can thus be defined as a vector:

$$e^{\beta h \sigma_i} = k_{\sigma_i} \equiv \begin{pmatrix} k_{+1} \\ k_{-1} \end{pmatrix} = \begin{pmatrix} e^{\beta h} \\ e^{-\beta h} \end{pmatrix}. \tag{9}$$

To represent the partition function of the square lattice as a tensor network we can place a g_{ijkl} tensor on each lattice site. This rank-4 tensor represents all possible states the site can be in and can be written as:

$$g_{ijkl} = k_i \delta_{ijkl}, \tag{10}$$

where $\delta_{ijkl} = 1$ if $i = j = k = l$ and $\delta_{ijkl} = 0$ otherwise. To simulate the interaction between the lattice sites, a Q matrix can be placed in between all lattice sites. The graphical notation for this network is shown in Figure 4a. It is now convenient to contract to a network with only a single tensor. This is done by taking the the square root and writing Q as the following:

$$Q_{\sigma_i, \sigma_j} = \sum_k \sqrt{Q}_{\sigma_i, k} \sqrt{Q}_{k, \sigma_j}, \tag{11}$$

which is essentially conducting the opposite of a contraction (Figure 4b). Finally, for representing Z with a network consisting of only one kind of tensor, each g_{ijkl} can be contracted with four $\sqrt{Q}$ matrices to obtain the following:

$$a_{ijkl} = \sum_s g_{ijkl} \sqrt{Q}_{is} \sqrt{Q}_{js} \sqrt{Q}_{ks} \sqrt{Q}_{ls}. \tag{12}$$

This tensor has shape $d \times d \times d \times d$, where d is defined as the number of spin states in the model ($d = 2$ for the Ising model). The partition function of the Ising model for a system size L with boundary conditions can thus be calculated by contracting a tensor network of $L \times L$ a_{ijkl} tensors.

2.5 Modifications for the Blume-Capel model

The Hamiltonian for the Blume-Capel model, defined in Equation 6, is identical to the Ising model Hamiltonian in Equation 1, except for the additional crystal-field term. This term is similar to the external magnetic field term, in the sense that it also contains the same, one index. The partition function for the Blume-Capel model is given by:

$$Z(\beta) = \sum_s e^{\beta J \sum_{<ij>} \sigma_i \sigma_j + \beta h \sum_i \sigma_i - \beta \Delta \sum_i \sigma_i^2} = \sum_s \prod_{<i,j>} e^{\beta J \sigma_i \sigma_j} \prod_i e^{\beta (h \sigma_i - \Delta \sigma_i^2)}. \tag{13}$$

Because of the addition of the 0 state, the new Q matrix is of shape 3×3:

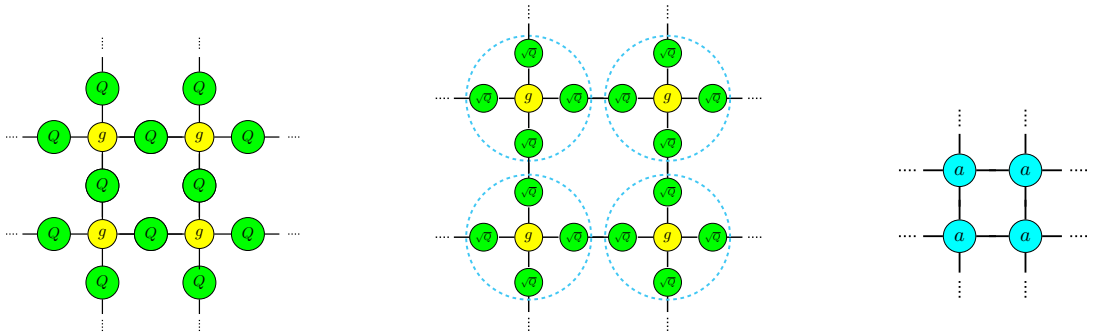

Figure 4: The steps involved in representing the partition function of the square lattice using solely a tensors. g tensors are positioned on each lattice site, while the interaction matrix Q is placed between adjacent sites (a). the matrix square root of each Q is obtained, leading to the presence of two $\sqrt{Q}$ matrices between neighboring lattice sites (b). Each g tensor is contracted with four $\sqrt{Q}$ tensors, resulting in a network comprising identical a tensors (c).

$$Q_{\sigma_i,\sigma_j} \equiv \begin{pmatrix} Q_{-1,-1} & Q_{-1,0} & Q_{-1,1} \\ Q_{0,-1} & Q_{0,0} & Q_{0,1} \\ Q_{+1,-1} & Q_{+1,0} & Q_{1,1} \end{pmatrix} = \begin{pmatrix} e^{\beta J} & 1 & e^{-\beta J} \\ 1 & 1 & 1 \\ e^{-\beta J} & 1 & e^{\beta J} \end{pmatrix}. \tag{14}$$

The new k vector also becomes three dimensional:

$$k_{\sigma_i} \equiv \begin{pmatrix} k_{-1} \\ k_0 \\ k_{+1} \end{pmatrix} = \begin{pmatrix} e^{-\beta(\Delta+h)} \\ 1 \\ e^{-\beta(\Delta-h)} \end{pmatrix}. \tag{15}$$

This finally yields an a tensor of shape $d \times d \times d \times d$, where $d = 3$ for the Blume-Capel model.

2.6 Finite size scaling

In the second order regime, the thermodynamic quantities m and ξ exhibit behavior that can be described by power laws. ξ is called the correlation length and is defined as the characteristic distance that two spins on different lattice sites are correlated. The power laws are derived by introducing the reduced temperature, defined as:

$$t = \frac{T - T_c}{T_c}. \tag{16}$$

The power laws for m and ξ are expressed as follows:

$$\xi \propto |t|^{-\nu}, \tag{17}$$

$$m \propto |t|^{\beta}. \tag{18}$$

The critical exponents ν and β characterize the behavior near the critical point for second order transitions, which belong to the 2D Ising universality class. According to [15], the exact solutions of the exponents in the 2D Ising universality class are given by $\nu = 1$ and $\beta = 1/8$.

The maximal correlation length ξ is directly proportional to finite size L (i.e., $\xi \propto L \propto t^{-\nu}$). By rearranging this relationship, we obtain the following expression:

$$T_c^*(L) = T_c + aL^{-1/\nu}. \tag{19}$$

In this equation, $T_c^*(L)$ represents the effective critical temperature corresponding to a finite size L, and a is a free parameter. This relationship shows that, when considering systems of finite size L for the Blume-Capel model in the second order regime and the Ising model, certain effects arise that impact the behavior of these models. These effects result in a deviation of T_c to a shifted T_c^* and impose limitations on ξ, which should diverge at T_c for systems of infinite size. The relationship in Equation 19 is hence particularly useful for approximating the critical temperature by extrapolating to the limit of $L \to \infty$ (i.e. $L^{-1/\nu} \to 0$).

In the Blume-Capel model, the addition of the crystal-field couplings term with parameter Δ introduces a new dimension to the phase diagram, and the same relation can be applied to the critical coupling parameter Δ_c and Δ_c^*:

$$\Delta_c^*(L) = \Delta_c + aL^{-1/\nu}. \tag{20}$$

Furthermore, Ref. [16] showed that a relationship can be established between m and L by starting with the following scaling ansatz:

$$m(t, L) = |t|^{\beta} \mathcal{F}(L/\xi), \tag{21}$$

where $\mathcal{F}$ represents an unknown function. Now using that $L \propto \xi \propto |t|^{-\nu}$, this can be rewritten as,

$$m(t, L) = L^{-\beta/\nu} \mathcal{F}(t \cdot L^{1/\nu}). \tag{22}$$

At $t = 0$, which means $T = T_c$, the function is constant, hence:

$$m(t = 0, L) \propto L^{-\beta/\nu}. \tag{23}$$

By taking the logarithm of both sides of this equation, we obtain:

$$\log\left[m(t = 0, L)\right] = -\frac{\beta}{\nu} \log L + b, \tag{24}$$

where b is a constant term. This relationship is useful, as it allows for the determination of the ratio of critical exponents β/ν by making a linear fit to data obtained for varying L.

3 Methods

This chapter begins by explaining the Corner Transfer Matrix Renormalization Group (CTMRG) method for approximating partition functions of infinite systems of the Ising and Blume-Capel models in Section 3.1. The following section, 3.2, describes how the CTMRG method can be used to approximate the partition function of a finite system with periodic boundary conditions. In Section 3.3 is explained, how to compute various thermodynamic properties, specifically the magnetization per site, correlation length, free energy, heat capacity, and magnetic susceptibility, using the results obtained from the CTMRG method. Section 3.4 discusses finite χ scaling and introduces relations analogous to those used in finite size scaling, which were discussed in Section 2.6. Finally, Section 3.5 explores the method of determining the tricritical point through correlation length extrapolation.

3.1 The Corner Transfer Matrix Renormalization Group method

In the Blume-Capel and Ising model, the partition function is obtained by contracting a network of a tensors, where each tensor represents a lattice site. The computation time of contracting the entire tensor network grows exponentially with the size of the network. The Corner Transfer Matrix Renormalization Group (CTMRG) method is an efficient approach to approximate this contraction and limit the computation time.

The goal of this method is to approximate an infinite network of a tensors as a network comprising four edge (T) and corner (C) tensors around one a tensor in the center. C and T are respectively of shapes $\chi \times \chi$ and $\chi \times \chi \times d$, where χ is called the bond dimension. The accuracy of this approximation can be systematically controlled with χ: the larger χ, the more accurate the approximation. Figure 5 illustrates the goal of the CTRMG method in graphical notation.

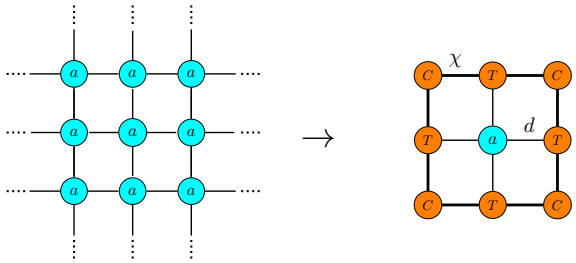

Figure 5: The goal of the CTMRG method: writing a network of a tensors, which represents the partition function of the system, as a network comprising corner (C) and edge (T) tensors around one a tensor in the center. In this network, the thick legs are of size χ and the thin legs of size d.

The idea of the CTRMG method is to start with randomly initialized C and T tensors, and then iteratively allow these tensors to converge to tensors that can collectively approximate the infinite network of a tensors. C and T are defined symmetric under the exchange of legs, which means $C_{ij} = C_{ji}$ and $T_{ijk} = T_{jik}$ where i and j are the legs of size χ. The iterations comprise adding a tensors in between the C and T tensors and the center a tensor. This network can be divided and contracted in four corners and edges respectively of shapes $\chi \times \chi \times d \times d$ and $\chi \times \chi \times d \times d \times d$ and consisting of the C and T tensors and the new a tensors, which is shown in Figure 6a. Renormalizing these corners and edges using the renormalization tensor $\tilde{U}^\dagger$, shown in Figure 6b and 6c, results in the same tensor network as before, but consisting of new corner and edge tensors C' and T' (Figure 6d). Because of rotational symmetry, these tensors only have to be computed once instead of four times and the same C' and T' can be inserted in each corner and edge.

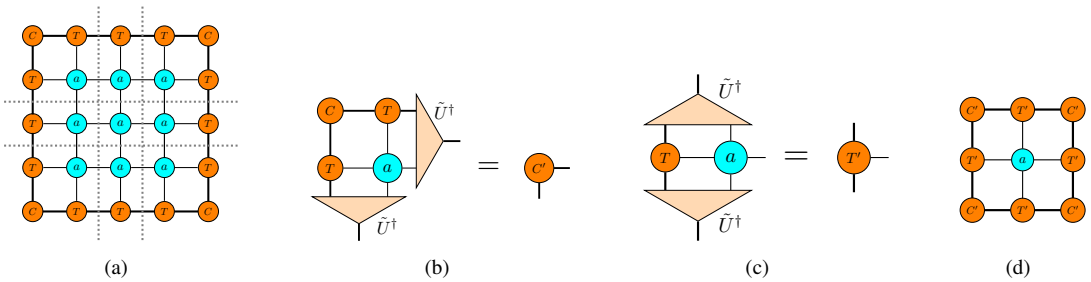

Figure 6: Steps for the CTM algorithm: addition of new a tensors and dividing the network in four corners and edges (a) renormalizing the corner (b) and edge (c) with the renormalization tensor $\tilde{U}^\dagger$ which results in shapes of respectively $\chi \times \chi$ and $\chi \times \chi \times d$ and yields a new network with C' and T' (d).

$\tilde{U}^\dagger$ is obtained by first contracting one corner, consisting of one C, two T, and an a tensor, to a tensor M of shape $\chi \times d \times \chi \times d$ and reshaping this tensor to a shape $\chi d \times \chi d$. M can be factorized with a singular value decomposition (SVD), giving:

$$M = U \cdot s \cdot V^\dagger, \tag{25}$$

where U and V are both unitary matrices and s is a diagonal matrix containing the singular values which are non negative and real in descending order. U, s and V are all of shape $\chi d \times \chi d$. The graphical notation of this SVD is shown in Figure 7. To obtain $\tilde{U}$, it is required to truncate U to shape $\chi d \times \chi$ and reshape to $\chi \times d \times \chi$. The truncation is done by only keeping the columns of U that correspond to the χ largest singular values. This choice ensures that the norm difference between M and the truncated $\tilde{M}$ is minimized. Renormalizing the corners and edges with $\tilde{U}^\dagger$ will yield a C' and T' respectively of shapes $\chi \times \chi$ and $\chi \times \chi \times d$. Contracting $\tilde{U}$ and $\tilde{U}^\dagger$ in the way shown in Figure 8 gives a rank-4 tensor which is approximately an identity matrix in each relevant subspace. Hence, renormalization with $\tilde{U}$ is approximately an isometric transformation and both the corners and edges can be renormalized with this same tensor .

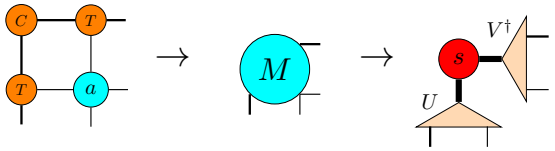

Figure 7: Graphical notation of the procedure for obtaining the U tensor. The first step is to contract one corner (consisting of one C, two T and an a tensor) to a tensor M of shape $\chi \times d \times \chi \times d$. Then a singular value decomposition as in Equation 25 can be conducted to obtain the U tensor of shape $\chi d \times \chi \times d$.

The reiteration of the steps described above is called the Corner Transfer Matrix (CTM) algorithm. In each iteration a new C' and T' is computed and both are normalized to keep numbers bounded. These steps can be repeated until convergence is reached, meaning:

$$\sum_k |s_k - s'_k| < \tau, \tag{26}$$

where s_k and s'_k are the vectors containing the normalized and truncated singular values of respectively C and C', and τ is some chosen tolerance. After convergence is reached, the tensor network in Figure 6d can be contracted to finally obtain an approximation of Z for an infinite system.

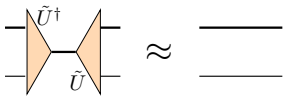

Figure 8: Graphical notation showing that the contraction of $\tilde{U}$ and $\tilde{U}^\dagger$ gives a rank-4 tensor which is approximately an identity matrix in the two subspaces.

3.2 Applying the Corner Transfer Matrix Renormalization Group method to finite systems

The CTM algorithm for the infinite system was discussed in the previous section. The algorithm for finite systems works in the same way, but has to be terminated when the desired system size L is reached. After one iteration the tensor network can be contracted to evaluate a 5×5 system, and thus after n iterations the contraction results in Z for an $(2n+3) \times (2n+3)$ system.

Open boundary conditions (OBC) can be implemented by initializing C and T in the first iteration of the algorithm with tensors C_b and T_b. C_b is defined as the contraction of a rank-2 g tensor (i.e $g_{ij} = k_i \delta_{ij}$) and two $\sqrt{Q}$ matrices resulting in shape $d \times d$. Contracting a rank-3 g tensor (i.e $g_{ijk} = k_i \delta_{ijk}$) and three $\sqrt{Q}$ matrices gives T_b, which has shape $d \times d \times d$. Both C_b and T_b are depicted in graphical notation in Figure 9a and 9b, respectively. The shapes of C_b and T_b differ from the shapes of C and T which are respectively given by $\chi \times \chi$ and $\chi \times \chi \times d$.

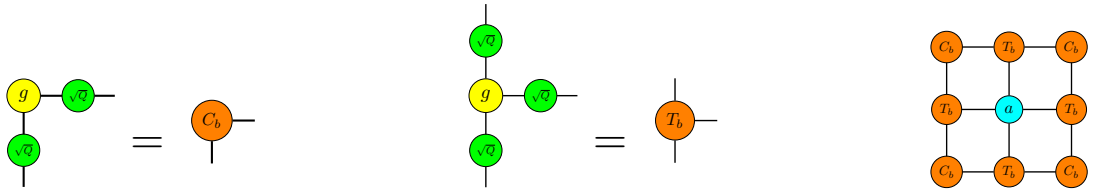

Figure 9: Corner and edge tensor C_b (a) and T_b (b) respectively of shapes $d \times d$ and $d \times d \times d$ and the initial tensor network (c) for evaluating a system with open boundary conditions.

In the case of an OBC system, it is necessary to implement a growth procedure for χ to avoid being constrained by a bond dimension of $\chi = d$. As previously stated, the bond dimension d takes on a value of 2 for the Ising model and 3 for the Blume-Capel model. χ can be grown to the desired value in the first few steps of the algorithm by keeping all columns of (i.e not truncating) U. As mentioned before, U has shape $\chi d \times \chi \times d$ and thus, not truncating U for n steps, yields a bond dimension of $\chi_n = d^{n+1}$. The desired bond dimension χ is then easily obtained by keeping χ columns of U after $\chi_n \geq \chi$.

3.3 Computing thermodynamic properties

3.3.1 Magnetization

The magnetization per site of the system m, defined in Equation 3, can be computed by dividing two tensor networks. The denominator equals the partition function defined in Section 3.1 and the numerator equals a similar network, but with a b tensor in the center. which is defined as:

$$b_{ijkl} = \sum_s s_i g_{ijkl} \sqrt{Q}_{is} \sqrt{Q}_{js} \sqrt{Q}_{ks} \sqrt{Q}_{ls}. \tag{27}$$

This tensor is equivalent to the a_{ijkl} tensor defined in Equation 12, except for the additional s_i factor. The division of the tensors to obtain m is shown in graphical notation in Figure 10.

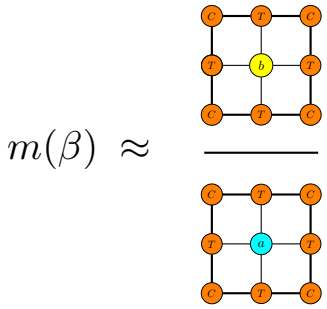

Figure 10: An approximation of the magnetization by dividing two tensor networks. The denominator is equivalent to the partition function defined in Section 3.1 (Figure 5) and the numerator is similar but with a b tensor in the center defined in Equation 27.

3.3.2 Correlation length

The correlation length ξ is defined as the maximum characteristic distance that two spins on different lattice sites are correlated. ξ can be computed using the contraction of two T tensors which is shown in graphical notation in Figure 11. Contracting and reshaping the T tensors yields T_M of shape $\chi^2 \times \chi^2$ which is known as the row-to-row transfer matrix. An eigenvalue decomposition can be conducted on T_M to obtain a vector with all eigenvalues in descending order λ_i. The correlation length is then defined as:

$$\xi = \frac{1}{\log\left(\lambda_1/\lambda_2\right)}, \tag{28}$$

Where λ_1 and λ_2 are respectively the largest and second largest eigenvalue.

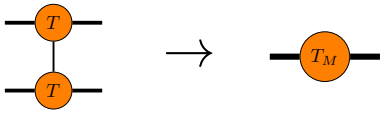

Figure 11: Contraction of two edge (T) tensors of shape $\chi \times \chi \times d$ and reshaping to T_M, the row-to-row transfer matrix, of shape $\chi^2 \times \chi^2$.

3.3.3 Free energy

The free energy f can be expressed by the following equation:

$$f = \frac{-k_B T \ln\left(Z\right)}{N} = -k_B T \ln\left(\kappa\right), \tag{29}$$

where N represents the number of lattice sites and $\kappa = Z^{1/N}$. In the limit as N approaches infinity, κ can be calculated as:

$$\kappa = \lim_{N \to \infty} Z^{1/N}. \tag{30}$$

Ref. [17] showed that this quantity can be obtained by performing division and multiplication operations using three tensor networks, which is shown in graphical notation in Figure 12.

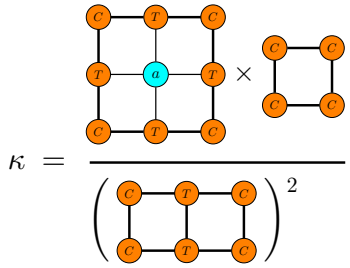

Figure 12: The value of κ is obtained through an approximation method that involves the division and multiplication of three tensor networks. The free energy f can be computed using Equation 29, which relates it to κ.

3.3.4 Heat capacity

The heat capacity is defined as the partial derivative of the energy per site with respect to temperature:

$$C = \frac{\partial E_s}{\partial T}, \tag{31}$$

where E_s is given by two times the bond energy E_b:

$$E_s = 2E_b = -2J\langle \sigma_i \sigma_j \rangle, \tag{32}$$

The notation $\langle \sigma_i \sigma_j \rangle$ denotes the average bond interaction between two lattice sites. In the case of a square lattice, each site is surrounded by four neighboring sites. However, it suffices to consider two bond interactions per site in order to account for all interactions. $\langle \sigma_i \sigma_j \rangle$ can be computed with the division of two tensors networks, which represent the spin interaction between two arbitrary sites in the infinite lattice and is shown in graphical notation in Figure 13.

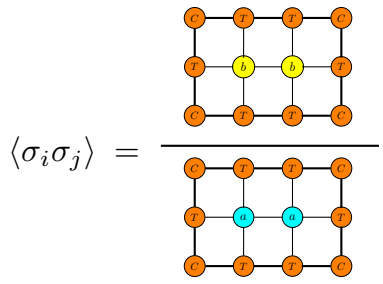

Figure 13: The division of two tensor networks, with the numerator comprising b tensors as defined in Section 3.3.1, and the denominator consisting of a tensors. The notation $\langle \sigma_i \sigma_j \rangle$ represents the spin interaction between two arbitrary lattice sites.

3.3.5 Magnetic susceptibility

The magnetic susceptibility χ_s provides information about the system's sensitivity or response to changes in the external magnetic field h in the vicinity of $h = 0$ and is defined as:

$$\chi_s \equiv \frac{\partial m}{\partial h}(h = 0) = \frac{m(h = \epsilon) - m(h = 0)}{\epsilon} \tag{33}$$

where ϵ is a small value (i.e. perturbation) of the external magnetic field. By taking the difference in magnetization between $h = \epsilon$ and $h = 0$ and dividing it by the magnitude of the perturbation (ϵ), we obtain the derivative of magnetization with respect to the external magnetic field around $h = 0$.

3.4 Finite χ scaling

In a similar manner to finite size effects, the presence of a finite bond dimension imposes limitations on the correlation length (ξ) and causes a shift in the critical temperature (T_c) to a new value denoted as $T_c^*(\chi)$. A similar relation to Equation 19 can be established for the second order regime by defining ξ_χ as the correlation length at $T_c^*(\chi)$:

$$T_c^*(\chi) = T_c + a\xi_\chi^{-1/\nu} \tag{34}$$

And similar to equation 20, exclusively for the Blume-Capel model in the second order regime, the same relation holds true between Δ_c and Δ_c^*:

$$\Delta_c^*(\chi) = \Delta_c + a\xi_\chi^{-1/\nu}. \tag{35}$$

3.5 Determination of the tricritical point by ξ-extrapolation

The point on the phase boundary that marks the border between the first order and second order regimes is known as the tricritical point (Δ_t, T_t). As discussed in Section 2.2, the second order transition is characterized by an infinite correlation length, whereas in the first order regime, the correlation length remains finite. The tricritical point can be determined by traversing along the first order line and employ finite χ scaling to extrapolate the correlation length ξ_χ to the limit of infinite χ. The tricritical point is then identified as the first point on the phase boundary where the extrapolated correlation length ξ reaches infinity. Ref. [18] introduces a new refinement parameter for extrapolations of the correlation length. This parameter is based on the eigenvalues of the row-to-row transfer matrix denoted as λ_i, as discussed in Section 3.3.2. By defining the following quantity:

$$\epsilon_i = -\log(\lambda_i), \tag{36}$$

the refinement parameter δ can be expressed as:

$$\delta = \epsilon_i - \epsilon_2, \tag{37}$$

where the eigenvalues $\epsilon_{i-1}, \epsilon_{i-2}, ...$ are either degenerate or nearly degenerate. Figure 14 provides a schematic representation of the ϵ spectrum of the transfer matrix. While the spectrum is discrete for finite values of χ, it becomes continuous in the limit as χ approaches infinity. This means that, for small i, the refinement parameter δ approaches zero in this limit. Substituting Equation 3.5 in the expression for the correlation length 3.3.2, gives the following:

$$1/\xi_\chi = \epsilon_2 - \epsilon_1 = \epsilon_2, \tag{38}$$

where the eigenvalues λ_i are normalized, so that the largest eigenvalue $\lambda_1 = 1$ and thus $\epsilon_1 = 0$.

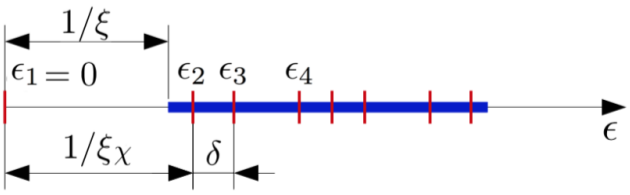

Figure 14: ϵ_i spectrum of the row-to-row transfer matrix T_M as shown in Figure 11. The discrete spectrum obtained with a finite χ is indicated by the red lines, while the blue band indicates the continuous spectrum in the $\chi \to \infty$ limit. $1/\xi_\chi$ is given by the distance between ϵ_1 and ϵ_2, whereas the correlation length ξ in the infinite χ limit is given by the gap between ϵ_1 and the onset of the continuous spectrum. $\delta = \epsilon_3 - \epsilon_2$ approaches 0 in the infinite χ limit. This figure is taken from [18] and edited by [19].

4 Results

The results for the Ising and Blume-Capel model are discussed in Section 4.1 and 4.2 respectively. All subsequent results presented in this chapter are obtained through simulations using the CTMRG method outlined in Section 3, where, for convenience, k_b and J are set to 1. Several thermodynamic properties as described in Section 3.3 for the Ising model and the Blume-Capel model are presented in this chapter. Specifically for the Ising model, results are presented concerning χ and size scaling, and are compared to exact solutions. Regarding the Blume-Capel model, the results presented focus on accuracy and comparisons with recent papers.

4.1 The Ising model

4.1.1 Thermodynamic properties

Figure 15 presents the relationship between the magnetization per site and temperature. The magnetization values were obtained through simulations performed for different values of χ, specifically 4, 8, 12, and 20. The method described in Section 3.3.1 was employed to calculate m within a temperature range of 2.23 to 2.30, with increments of 0.0001. A convergence criterion $\tau = 10^{-10}$ was chosen. For comparison, the exact solution, as provided in Equation 5, has also been included in Figure 15. This enables a visual assessment of the agreement between the calculated magnetization values obtained from simulations and the theoretical solution.

Finite χ imposes a cutoff in the correlation length, and this cutoff has a more pronounced effect on smaller χ values, leading to less accurate results. This phenomenon is evident in Figure 15, where the exact solution is approached as the bond dimension increases.

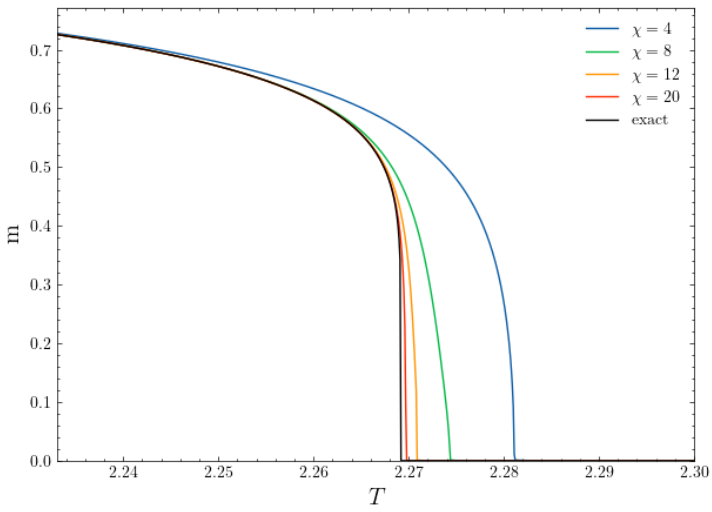

Figure 15: Magnetization (m) as a function of temperature (T) for the Ising model. Simulations were conducted for various values of χ (4, 8, 12, and 20), and the magnetization was computed using the methodology described in Section 3.3.1. The exact solution is depicted by the black curve.

Figure 16a presents the correlation length (ξ) as a function of T for different values of χ (4, 8, 12, and 20). The same converged tensors used for computing the magnetization, as described above, were employed to determine ξ as a function of T. The correlation length was computed with the method outlined in Section 3.3.2. Consistent with expectations, increasing χ results in a sharper and higher peaks in ξ, and the maximum of the peak shifts closer to the exact critical temperature (T_c), indicated by

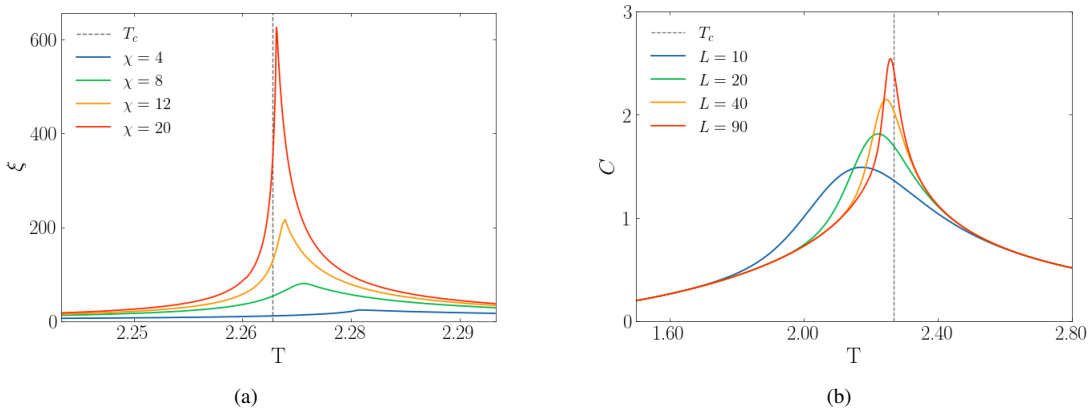

Figure 16: Correlation length for varying bond dimension χ (a) and heat capacity for varying system size L (b) as a function of T. The correlation length was computed as described in Section 3.3.2 and the heat capacity as described in Section 3.3.4. Periodic boundary conditions were employed in the finite system.

a black dotted line. This observation highlights that finite χ imposes a cutoff in the correlation length and leads to a shift of T_c to T_c^*, as discussed in Section 3.4.

Heat capacity C as a function of T for different system sizes L (10, 20, 40, and 90) is shown in Figure 16b. In each system, open boundary conditions were utilized using initial edge and corner tensors, specifically described in Section 3.2. The method discussed in Section 3.3.4 was used to compute the heat capacity. The temperature ranges from 1.5 to 2.8 with increments of 0.001. To minimize the influence of finite χ effects and emphasize the impact of finite L effects, a relatively large bond dimension of 24 was selected. It is observed that as the system size (L) increases, the heat capacity peak becomes more prominent and sharper, similar to the behavior of the correlation length with increasing χ.

The free energy f as function of temperature T is shown in Figure 17. The temperature range considered spans from 0.55 to 3.4, with increments of 0.01, while a value of $\tau = 10^{-9}$ was selected. The simulations were performed for different values of χ, specifically 4, 8, and 16. f was computed following the methodology described in Section 3.3.3. The curves corresponding to different values of χ exhibit significant overlap, indicating that finite χ effects have a limited impact on the accuracy of f.

4.1.2 Scaling

As discussed in Section 2.6 and 3.4, L and ξ_χ follow similar relationships between T_c and T_c^* (resp. Equation 19 and 34). Both these relationships, along with obtained data, were employed to estimate T_c. The exact solution provided by [15] is $T_c = 2/\ln(1+\sqrt{2}) \approx 2.2691853$. For both finite size and χ scaling the exact value $\nu = 1$ was used in a fit of obtained data. The determination of the critical temperature using these two methods, finite size scaling and χ scaling, allows for a direct comparison between the two approaches.

For finite χ scaling, simulations were run for various χ, specifically 4, 8, 12, 16, and 24. A step size in temperature of 0.00005 and $\tau = 10^{-8}$ were chosen. The location and height of the correlation length peaks as functions of temperature were used to determine $T_c^*(\chi)$ and $(\xi_\chi^{eff})^{-1/\nu}$. By fitting Equation 34 to the obtained data, a critical temperature of $T_c = 2.2695(2)$ was determined. The data and the fit for finite χ scaling are shown in Figure 18a.

Simulations were run for system sizes of 50, 70, 90 and 150. A step size in temperature of 0.01 and

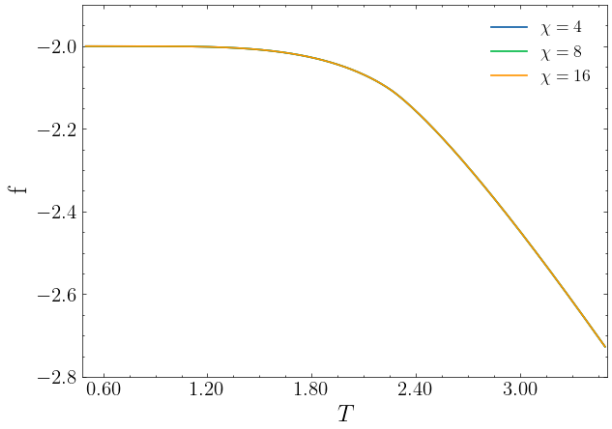

Figure 17: Free energy (f) as a function of temperature (T) for the Ising model. Simulations were conducted for various values of χ (4, 8, and 16), and the free energy was computed using the methodology described in Section 3.3.3.

$\tau = 10^{-9}$ was chosen. The location of the heat capacity peaks was used to determine the location of T_c^*. Fitting Equation 19 yielded a critical temperature of $T_c = 2.269(1)$. The fit and data for the finite size analysis are presented in Figure 18b.

Furthermore, the ratio of critical exponent β/ν was determined using finite size scaling and Equation 24. The correlation length for the converged tensors with a convergence criterion $\tau = 10^{-11}$ at $t = 0$ (i.e. $T = T_c = 2/\log(1+\sqrt{2})$) was determined for varying χ, specifically 12, 14, 16, 18, 20, 22, and 24. A fit to Equation 19 yielded a ratio of the critical exponents of $\beta/\nu = 0.125(1)$.

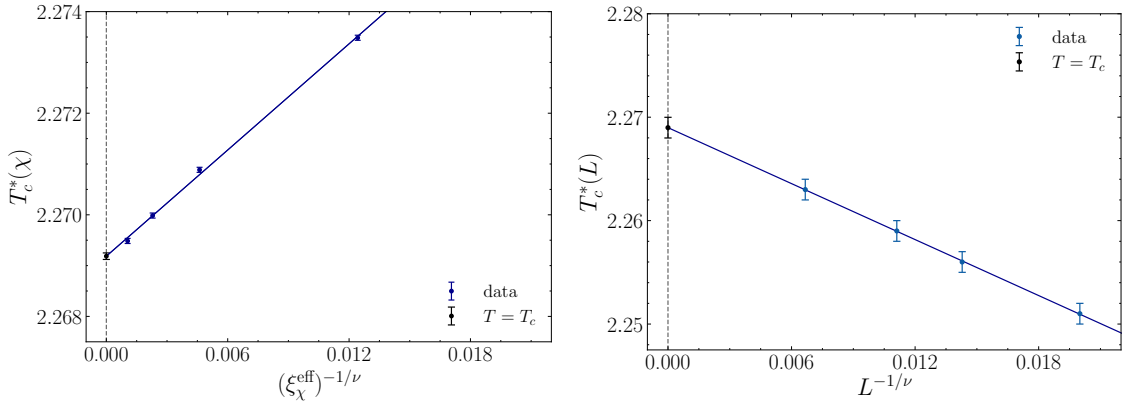

(a) (b)

Figure 18: Finite χ scaling fit to Equation 34 (a) and finite size scaling fit to Equation 19 (b). The exact value of the critical exponent, $\nu = 1$, was used. The error bar on the data is determined by the step size in temperature of the simulation, respectively 0.00005 and 0.01 for finite χ and size scaling. The obtained critical temperatures, $T_c = 2.2695(2)$ and $T_c = 2.269(1)$, are indicated with a black data point in both graphs.

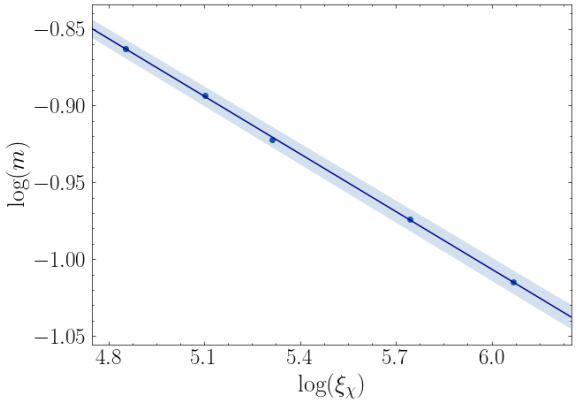

Figure 19: Fit of the acquired data for varying χ (12, 14, 16, 18, 20, 22, 24) to an equation of the form described by Equation 19: $-a \log(x) + b$. The resulting fit provides a value of $a = \beta/\nu = 0.125(1)$, where the error in the slope a is visually represented using a transparent blue color.

4.2 The Blume-Capel model

4.2.1 Thermodynamic properties

Figure 20a illustrates the dependency of the magnetization m on Δ, where the increments of Δ are set at 0.0005. The graph displays two scenarios: one with an external magnetic field of $h = 0$ and the other with $h = 10^{-6}$, while χ takes values of 4, 8, and 24. The dashed line in Figure 20a represents the magnetization for the system with $h = 10^{-6}$. The temperature was fixed at $T = 1.4$, which is in the second order regime, and a tolerance of $\tau = 10^{-9}$ was applied. In Figure 20b, the magnetic susceptibility χ_s is depicted as a function of Δ. The computation of χ_s was carried out using Equation 33 with a value of $\epsilon = 10^{-6}$. Notably, both graphs exhibit an increasing response to the small external magnetic field h as the value of the bond dimension χ increases. This phenomenon arises from the larger correlation length observed with increasing values of χ, indicating a spin correlation over an extended characteristic distance. Consequently, the response to the external magnetic field becomes more pronounced.

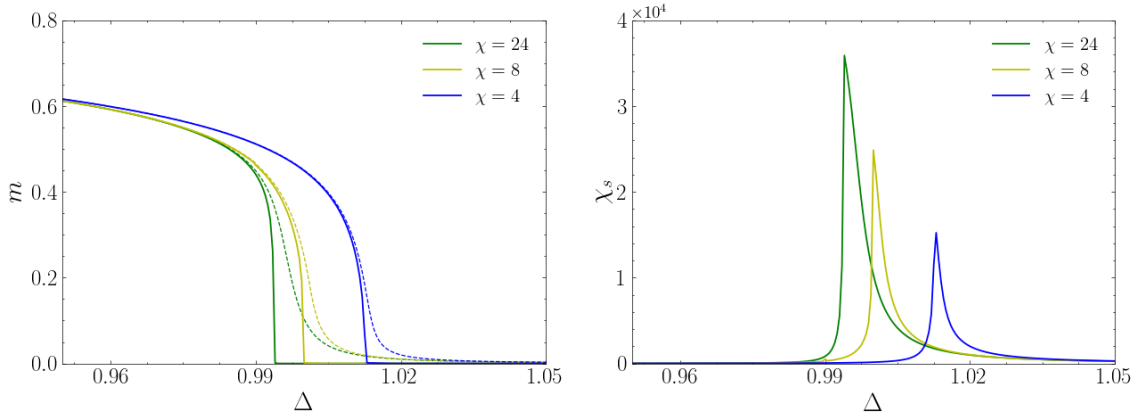

Figure 20: m without external magnetic field $h = 0$, indicated by the solid line, and for a small external field $h = 10^{-6}$, indicated by the dashed line (a), and magnetic susceptibility χ_s (b) as a function of Δ for varying χ (4, 8, 24). The computations for m and χ_s were performed using the methodologies outlined in Sections 3.3.1 and 3.3.5, respectively.

The correlation length ξ and heat capacity C as function of T for varying Δ, specifically 0, 0.5, 1, and 1.5 are presented in Figure 21. Increments in T are 0.001, the convergence criterion $\tau = 10^{-9}$, and χ is chosen to be 16. ξ and C are computed using the method described in Section 3.3.2 and 3.3.4, respectively. Note that the specific heat peak increases in height for increasing Δ. This is because the number of zero states, which are associated with a lack of spin interactions between the ± 1 states, also increases with Δ. As discussed in Section 3.3.4 the heat capacity is given by the derivative of the energy per site: $C = \partial E_s / \partial T$. The energy per site E_s in regions with a greater abundance of zero states is more sensitive to temperature changes, which leads to a higher peak and an overall larger heat capacity.

The correlation length peaks show similar heights across different values of Δ. However, there is a slight variation in the peak heights. This can be attributed to the narrow width of the correlation length peak. The peak is characterized by a thin and sharp profile, making it prone to missing the highest maximum when the temperature increment is too large. In theory, the correlation length and the heat capacity are both expected to diverge at the critical temperature of the transition. However, as elaborated in Section 3.4, finite χ introduces a limitation on the extent of the correlation length and the heat capacity.

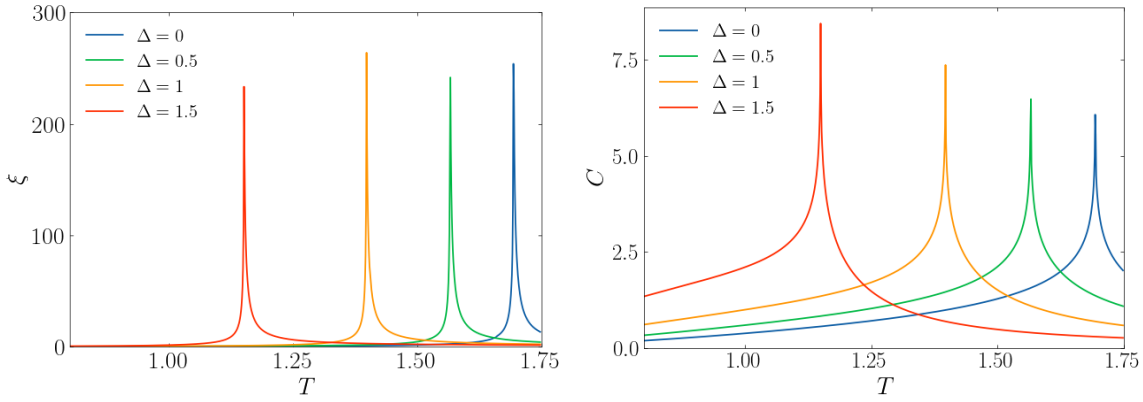

Figure 21: The correlation length ξ (a) and heat capacity C (b) as a function of temperature for varying values of the coupling parameter Δ (0, 0.5, 1, 1.5). ξ and C were computed following the methods in Section 3.3.2 and 3.3.4, respectively.

The free energy f as a function of Δ for a temperature of $T = 0.5$, in the vicinity of the first order transition between the ferromagnetic (F) and paramagnetic (P) state, is presented in Figure 22. The plot includes the free energy curves for different values of χ (4, 10, 32) with increments in Δ of 0.0001. Both the approach from the right and the left are presented. In the context of the CTMRG method, this means that the initial corner and edge tensors are initialized with the converged tensors from the previous Δ step.

As discussed in Section 2.2, hysteresis occurs during first-order phase transitions. This phenomenon is evident in the overlapping regions between the solutions obtained from the right and left approaches, where the free energy remains in either the P or F state for a longer period. The point of intersection between these two solutions defines the transition point in the first-order regime. Note that for increasing χ, f stays in the corresponding solution for a longer duration. This behavior can be understood by considering the increasing number of CTM steps as the bond dimension χ increases. With higher χ values, the tensors require more iterations to converge, leading to a greater probability of transitioning between the two solutions.

4.2.2 Critical exponent

The shift of the location of the peak for varying system size L with boundary conditions employed is illustrated in Figure 23a at a temperature $T = 1.4$ and for bond dimension $\chi = 16$. Δ was varied with increments of 0.002 and a tolerance of $\tau = 10^{-9}$ was chosen. The specific heat was computed following the methodology discussed in Section 3.3.4. The figure shows that the location of the peak shifts and the height, which should diverge for $\chi \to \infty$, increases with increasing system size L.

The critical exponent ν is determined using finite size scaling with the locations of the specific heat peaks. Simulations were run for varying L, specifically 10 to 55 with increments of 5. A bond dimension of $\chi = 16$, a convergence criterion of $\tau = 10^{-9}$, and a step size in Δ of 0.001 was utilized. A fit to the relationship between Δ_c and Δ_c^* as a function of L (Equation 20) gave $\nu = 1.01(4)$. This value agrees with the exact value of 1 in the 2D Ising universality class, defined in Section 2.6. The obtained critical coupling parameter is given by $\Delta_c = 0.994(3)$.

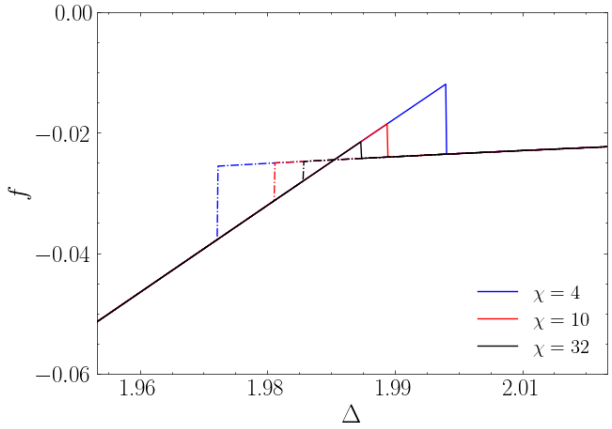

Figure 22: The free energy f as a function of Δ at the first order phase transition with $T = 0.5$ and for various χ (4, 10, 32). The solid line represents an approach from the left and the dashed line an approach from the right.

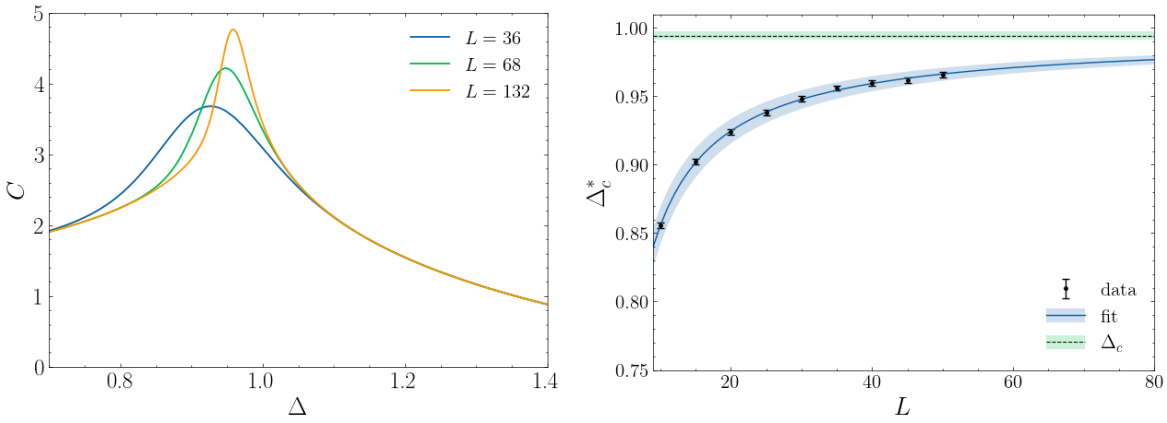

(a) (b)

Figure 23: The heat capacity as a function of Δ for system sizes 36, 68 and 132 (a) and a fit of Equation 20 to the locations of the heat capacity peaks Δ_c^* as a function of system sizes from $L = 10$ to $L = 55$ with increments of 5 (b). The fit provides a value of $\nu = 1.01(4)$ and $\Delta_c = 0.994(3)$. The errors on ν and Δ_c are displayed with respectively the blue and gray transparent colors.

4.2.3 Phase diagram

The phase diagram of the Blume-Capel model in the Δ, T plane is presented in Figure 24. The phase diagram provides values from two recent papers [20, 9]. The numerical values of all points in the phase diagram are summarized in Table 1. Points in the second order regime were obtained by finite χ scaling, equivalent to the method described in Section 4.1.2. Vertical cuts were made, i.e. keeping Δ constant and varying T, where the maximum of the correlation length peak ξ^{eff} was determined for varying χ (6, 8, 12, 16, 20, 26). In Figure 25a the fit to Equation 34 is shown for $\Delta = 1$ and an accuracy comparison with [20] is provided. The obtained value for the critical temperature is $T_c = 1.39731(5)$ and provides an improvement of two decimal points compared to [20].

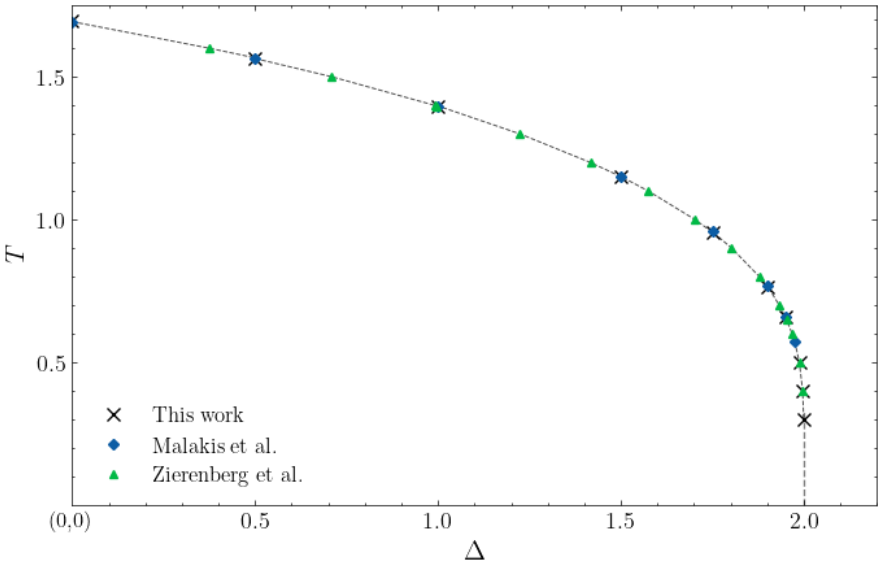

Figure 24: Phase diagram of the Blume-Capel model in the Δ, T plane. Data of two other recent works [20, 9] are provided. All individual points are summarized in Table 1.

The points within the first order regime were obtained by identifying the intersection between the left and right approach of the transition. This was accomplished by performing horizontal cuts in the phase diagram while keeping T constant and varying the parameter Δ. A relatively small bond dimension of $\chi = 16$ was chosen, as the finite effects associated with $\chi \geq 10$ were found to be on the order of 10^{-10}. For one specific critical coupling parameter Δ_c, at a temperature of $T = 0.5$, an increased level of accuracy was pursued, reaching 10^{-9}. This was achieved by evaluating two points on both sides of the intersection for both the right and left approach. By interpolating between these points, a precise value for Δ_c was obtained, yielding $\Delta_c = 1.987885768(3)$. The corresponding graph depicting the intersection between the two transitions is displayed in Figure 25b, showcasing an enhancement of three decimal points compared to recent work by [9].

For determining the tricritical point, vertical cuts were made within the first order regime for temperatures that approach the tricritical point. A step size in Δ of 0.000005 and a convergence criterion of $\tau = 10^{-9}$ was used for these cuts. The cuts were performed from both the left and right approach. The intersection between the free energy of the approaches was determined to obtain Δ_c. For each point along the first order boundary that approached the tricritical point, the methodology outlined in Section 3.5 was applied to determine the correlation length in the $\chi \to \infty$, or equivalently, the $\delta \to 0$ limit. The extrapolation for a point close to the tricritical point, $(\Delta = 1.9661, T = 0.6075)$, is shown in Figure

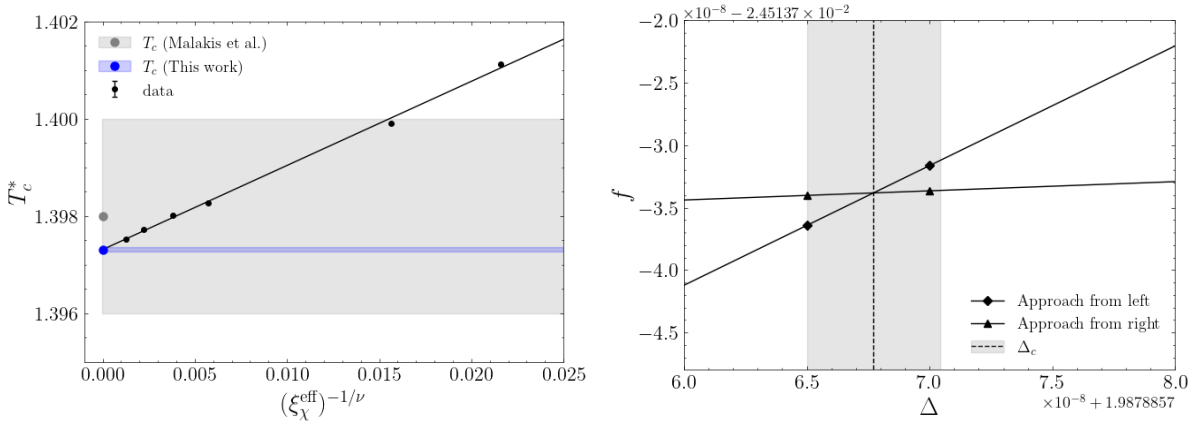

(a) (b)

Figure 25: Graphs showcasing the methods of obtaining critical points in both segments of the phase diagram. (a) shows the fit to Equation 35 for correlation length peaks at $\Delta = 1$ and for various χ values, specifically 6, 8, 12, 16, 20, and 26. The exact value of the critical exponent, $\nu = 1$, was used. The critical temperature was estimated to be $T_c = 1.39731(5)$, which is then compared to the estimate provided by [20], $T_c = 1.398(2)$. The shaded regions in different colors represent the corresponding uncertainties. (b) shows the intersection of the two approaches for $T = 0.5$, where the accuracy was pushed to the order of 10^{-9}. The estimated critical coupling parameter is given by $\Delta_c = 1.987885768(3)$, compared to $\Delta_c = 1.987889(5)$ presented by [9].

26a, for varying χ between 16 and 32 with steps of 2.

This extrapolation was conducted for ten specific points on the phase boundary in the vicinity of the tricritical point. The resulting extrapolated values of ξ against T for these points are shown in Figure 26. Through a visual examination of the graph, it can be concluded that the temperature of the tricritical point is determined to be $T_t = 0.6079(1)$. The error bar is defined by considering the two points positioned to the left and right of this temperature. The corresponding Δ is given by $\Delta_t = 1.96600(1)$, where the error bar is defined by the step size of the vertical cuts. Hence, the estimated tricritical point is given by

$$[\Delta_t = 1.96600(1), T_t = 0.6079(1)].$$

All ten points corresponding to Figure 26b are summarized in Table 2.

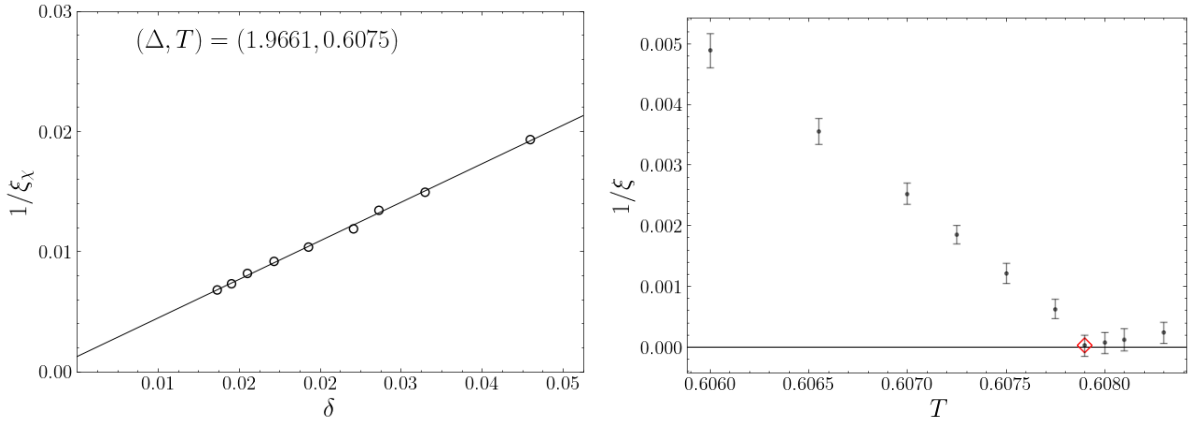

(a) (b)

Figure 26: (a) shows the ξ-extrapolation of a specific point, $(\Delta = 1.9661, T = 0.6075)$, on the first order boundary close to the tricritical point (Δ_t, T_t). (b) displays the extrapolated $1/\xi$ for ten points approaching the tricritical point. Each datapoint is obtained for $\chi = 16$ to $\chi = 32$ with increments of 2 and a convergence criterion of $\tau = 10^{-9}$. The estimate for the tricritical point is indicated with the red diamond and is given by $[\Delta_t = 1.96600(1), T_t = 0.6079(1)]$.

		This work		Malakis et al. [20]	Zierenberg et al. [9]
Δ	T	T	Δ	T	Δ
0		1.69397(3)		1.693(3)	
	1.6				0.375(2)
	1.5				0.7101(5)
0.5		1.5663(2)		1.564(3)	
	1.4				0.9909(4)
	1.398				0.9958(4)
1		1.39731(5)		1.398(2)	
	1.3				1.2242(4)
	1.2				1.4167(2)
1.5		1.15055(1)		1.151(1)	
	1.1				1.5750(2)
	1.0				1.70258(7)
1.75		0.9560(1)		0.958(1)	
	0.9				1.80280(6)
	0.8				1.87879(3)
1.9		0.7650(4)		0.769(1)	
	0.7				1.93296(2)
1.95		0.65762(8)		0.659(2)	
	0.65				1.95273(1)
	0.6				1.968174(3)
	0.5		1.987885768(3)		1.987889(5)
	0.4		1.9968(1)		1.99683(2)
	0.3		1.9996(1)		

Table 1: Values that represent the points in the phase diagram (Figure 24). The first two columns indicate whether Δ or T was varied to obtain the corresponding T or Δ of the critical point, respectively. The values within parentheses indicate the error in either Δ or T.

T	Δ	$1/\xi$
0.606	1.96653(1)	0.00489(28)
0.60655	1.96638(1)	0.00355(21)
0.607	1.96626(1)	0.00252(17)
0.60725	1.96619(1)	0.00185(15)
0.6075	1.96612(1)	0.00122(17)
0.60775	1.96605(1)	0.00063(15)
◇ 0.6079(1)	1.96600(1)	0.00002(18)
0.608	1.96598(1)	0.00006(18)
0.6081	1.96595(1)	0.00012(18)
0.6083	1.96589(1)	0.00024(18)

Table 2: Values corresponding to the points in Figure 26b. The first column represents the temperature T of the vertical cut in the phase diagram, the second column the corresponding Δ value at the intersection of the right and left approach, and the third column provides the extrapolated inverse correlation length $1/\xi$. The estimate for the tricritical point is indicated with the red diamond.

5 Discussion and Conclusion

In this work, both the Ising model and the Blume-Capel model were studied using a tensor network approach and the Corner Transfer Matrix Renormalization Group (CTMRG) method. This powerful method enables the approximation of the partition function for both models, where the accuracy can be controlled by the bond dimension χ. The goal of this thesis was to compare the CTMRG results for the Ising model to exact results, and compare the results for the Blume-Capel model to recent studies that employed alternative methodologies.

Results for the Ising model were presented in Section 4.1. Firstly, the thermodynamic properties magnetization, correlation length, heat capacity, and free energy were studied. A comparison was made between the obtained magnetization and the exact solution, revealing that the method can produce results close to the exact solution. Furthermore, finite χ and size scaling were employed for determining the critical temperature of the Ising model. The obtained critical temperatures are given by

$$T_c^{\text{Ising}} = 2.2695(2) \text{ for finite } \chi \text{ scaling, and}$$

$$T_c^{\text{Ising}} = 2.269(1) \text{ for finite size scaling.}$$

Both results agree with the exact value given by $T_c^{\text{exact}} = 2.2691853....$

Additionally for the Ising model, finite χ scaling was employed to estimate the ratio of the critical exponents. A fit to Equation 24, yielded

$$\beta/\nu = 0.125(1),$$

which agrees with the exact value defined in Section 2.6, $\beta/\nu = 0.125$.

In Section 4.2 the CTMRG method was applied to the Blume-Capel model and the results presented. First of all, thermodynamic properties in the second order regime were studied, specifically magnetization per site, magnetic susceptibility, correlation length, and heat capacity. The free energy was studied in the first order regime, which showed hysteresis effects. Next, finite size scaling using the shift of the heat capacity peaks was employed to estimate the critical exponent ν. A fit to Equation 20, yielded

$$\nu = 1.01(4).$$

This estimate agrees with the exact value of $\nu = 1$, defined in Section 19. The error on this value is relatively large and can be attributed to the limited amount of data points. The fit can be improved when considering more data points, and would yield a critical exponent ν with a smaller error.

In addition, results focusing on accuracy and comparisons to recent papers were presented for the Blume-Capel model. The phase diagram in the Δ, T plane was presented in Figure 24 and the corresponding points summarized in Table 1. Vertical cuts were made to obtain the points on the second order phase boundary. One specific critical temperature corresponding to $\Delta = 1$ obtained through this work and the estimate from [20] are given by

$$\text{this work: } T = 1.39731(5),$$

$$\text{Malakis et al. [20]: } T = 1.398(2).$$

The estimated temperature agrees with the value from [20] and presents an improvement in accuracy of two decimal points. The temperatures in the second order regime are obtained through finite χ scaling of the correlation length peaks ξ_χ^{eff}. Ref. [20] employed Wang-Landau simulations to investigate the

Blume-Capel model, which comprises Monte Carlo (MC) sampling and iterative updates of the density of states to determine the model's thermodynamic properties.

For a specific point on the first order phase boundary the accuracy was pushed to the order of finite χ effects, 10^{-10} for $\chi \geq 10$. The intersection was determined between the left and right approaches for varying Δ and constant temperature $T = 0.5$. The corresponding Δ and the estimate from [9] are given by

$$\text{This work: } \Delta = 1.987885768(3),$$

$$\text{Zierenberg et al. [9]: } \Delta = 1.987889(5).$$

Ref. [9] utilized MC simulation methods to study the phase diagram of the 2D Blume-Capel model. The improved accuracy demonstrates the remarkable capability of the CTMRG method, as it enables relatively high precision to be achieved within short computational times and with limited computing power.

The tricritical point (Δ_t, T_t) was estimated by performing ξ extrapolation with refinement parameter δ. The extrapolated correlation lengths for points approaching the tricritical point along the first order phase boundary were presented in Figure 26 and summarized in Table 2. The estimated values of the tricritical point, where $1/\xi$ extrapolates to zero, are as follows:

$$[\Delta_t = 1.96600(1), T_t = 0.6079(1)].$$

This estimate is consistent with other studies. Estimates include, MC simulations with field mixing, $[\Delta_t = 1.9665(3), T_t = 0.608(1)]$ [10] and $[\Delta_t = 1.9665(3), T_t = 0.608(1)]$ [11], and Wang-Langdau simulations, $[\Delta_t = 1.966(2), T_t = 0.609(3)]$ [12] and $[\Delta_t = 1.9660(1), T_t = 0.6080(1)]$ [13]. Although the accuracy already stands among the highest in these recent studies, it could still be improved by considering more horizontal cuts in the first order phase boundary in the vicinity of the tricritical point and utilizing smaller step sizes in Δ. In addition, the number of χ values could be increased in the ξ-extrapolation.

Acknowledgements

I would like to thank dr. Philippe Corboz and Yining Zhang MSc for their supervision, feedback, and for the weekly meetings. I would like to thank dr. Edan Lerner for examining my project.

References

[1] T. Nishino and K. Okunishi. Corner transfer matrix renormalization group method. *Journal of the Physical Society of Japan*, 65(4):891–894, apr 1996.

[2] R. Orús. A practical introduction to tensor networks: Matrix product states and projected entangled pair states. *Annals of physics*, 349:117–158, 2014.

[3] W. Lenz. Beitrag zum verständnis der magnetischen erscheinungen in festen körpern. *Z. Phys.*, 21:613–615, 1920.

[4] E. Ising. Contribution to the theory of ferromagnetism. *Z. Phys*, 31(1):253–258, 1925.

[5] M. Blume. Theory of the first-order magnetic phase change in uo2. *Physical Review*, 141(2):517, 1966.

[6] H. W. Capel. On the possibility of first-order phase transitions in ising systems of triplet ions with zero-field splitting. *Physica*, 32(5):966–988, 1966.

[7] M. Blume, V. J. Emery, and R. B. Griffiths. Ising model for the λ transition and phase separation in he 3-he 4 mixtures. *Physical review A*, 4(3):1071, 1971.

[8] L. Onsager. Crystal statistics. i. a two-dimensional model with an order-disorder transition. *Physical Review*, 65(3-4):117, 1944.

[9] J. Zierenberg, N. G. Fytas, M. Weigel, W. Janke, and A. Malakis. Scaling and universality in the phase diagram of the 2d blume-capel model. *The European Physical Journal Special Topics*, 226(4):789–804, 2017.

[10] N. B. Wilding and P. Nielaba. Tricritical universality in a two-dimensional spin fluid. *Physical Review E*, 53(1):926, 1996.

[11] J. A. Plascak and P. H. L. Martins. Probability distribution function of the order parameter: Mixing fields and universality. *Computer Physics Communications*, 184(2):259–269, 2013.

[12] C. J. Silva, A. A. Caparica, and J. A. Plascak. Wang-landau monte carlo simulation of the blume-capel model. *Physical Review E*, 73(3):036702, 2006.

[13] W. Kwak, J. Jeong, J. Lee, and D. Kim. First-order phase transition and tricritical scaling behavior of the blume-capel model: A wang-landau sampling approach. *Physical Review E*, 92(2):022134, 2015.

[14] P. D. Beale. Finite-size scaling study of the two-dimensional blume-capel model. *Physical Review B*, 33(3):1717, 1986.

[15] J. M. Yeomans. *Statistical mechanics of phase transitions*. Clarendon Press, 1992.

[16] L. Wang. *Computational studies of quantum spin systems*. 2010.

[17] R. J. Baxter. Variational approximations for square lattice models in statistical mechanics. *Journal of Statistical Physics*, 19(5):461–478, 1978.

[18] M. M. Rams, P. Czarnik, and L. Cincio. Precise extrapolation of the correlation function asymptotics in uniform tensor network states with application to the bose-hubbard and xxz models. *Physical Review X*, 8(4):041033, 2018.

[19] R. van der Werff. Simulating classical spin systems using the fixed point corner method. Master's thesis, University of Amsterdam, 2018.

[20] A. Malakis, A. N. Berker, I. A. Hadjiagapiou, N. G. Fytas, and T. Papakonstantinou. Multicritical points and crossover mediating the strong violation of universality: Wang-landau determinations in the random-bond d= 2 blume-capel model. *Physical Review E*, 81(4):041113, 2010.